Small-Disturbance Angle Stability Control With High Penetration of Renewable Generations

Nadarajah Mithulananthan, *Senior Member, IEEE*, Rakibuzzaman Shah, *Student Member, IEEE*, and Kwang Y. Lee, *Fellow, IEEE*

***Abstract*—Growth and penetration of renewable energy has been remarkable during the last few years in many power systems around the world. Essentially, there are two major technologies responsible for the growth, namely wind and photovoltaic. The technologies involved in harnessing energy from wind and sun are distinctly different in dynamic characteristics and limitations. Consequently, their influence on stability of power system should not be overlooked. This paper examines the small-disturbance angle stability with high penetration of renewable energy and proposes a methodology to control. The hierarchical principal component analysis, which is a clustering method corresponding to the eigenvalue sensitivity of reactive power control, is utilized to select the renewable generator clusters for different reactive power control scheme. Then, the framework based on structured singular value has been employed, in which the reactive power controls of renewable generator clusters are selected such that the desired robust stability criterion is satisfied. Results obtained in 16-machine 68-bus test system (typically used for small-signal angle stability studies) show the effectiveness of the proposed methodology.**

***Index Terms*—Clustering method, photovoltaic (PV) generation, reactive power management, small-disturbance angle stability, structured singular value (SSV), wind generation.**

I. Introduction

In recent years, the need for clean energy in an effort to reduce emissions and minimize our reliance on fossil fuels has led to worldwide integration of large-scale renewable generations [1]–[5]. In 2009, European Union Renewable Energy Directive set a target of generating over 32% of total power from renewable energy by 2030, with a target of 100% by 2050 [2]. In addition, following the energy sector regulation in Canada, the U.S., China, India, and Australia, renewable energy generators ranging from 10 to 250 MW and above are either already embedded or expected to be integrated into the transmission network in the near future [1]–[5]. Until recently, wind power plants (WPPs), together with photovoltaic power plants (PPPs), are the widely used renewable energy sources for electricity. At the current commissioning rate, WPPs and PPPs could count for 50% of the total system capacity of some utilities in the foreseeable future.

The structural changes in power systems due to the proliferation of wind and photovoltaic (PV) resources present notable concerns regarding reliable and secure operation of power system, and one of the major concerns regarding secure operation is small-disturbance angle stability. In the recent past, there has been an immense effort in investigating the impact of increased penetration of WPPs and PPPs on power-system small-disturbance angle stability [6]–[10]. Some previous research efforts (e.g., [6] and [7]) have investigated the impact of a fixed-speed wind turbine on power-system small-disturbance angle stability. Several wind turbine technologies have evolved in recent years, including the doubly-fed induction generator (DFIG) and the fast growing full-converter wind turbine technologies. Among them, the market share analysis has shown that DFIG shared 55%–60% of the wind turbine market in 2011 [11], [12], and the market share forecasting reveals that integration of wind farms all over the world will continue to be based on the DFIG technology along with full converters [12]. Therefore, this paper has focused on DFIG-based WPPs; incidentally, the control philosophy of full converter technology and the PV generator generic model are almost identical from the grid side of the system.

Gautam and others [8] show that the increased penetration of DFIG-based wind generations could have both beneficial and adverse effects on small-disturbance angle stability. Moreover, results in [9] and [10] depict that the power system with increased PV penetration could be vulnerable to small-disturbance angle stability. As wind and PV generators have very little or no inertia, integration of these types will reduce the effective inertia of the system. In a reduced inertia system following a disturbance, the effective aggregated angular acceleration of synchronous generators could be high, requiring a larger restoring force to return the machines to equilibrium. Carrying this extra burden would stress the synchronous units that coexist with the renewable generations and could lead to a less secure system operation in terms of rotor angle stability [13]. The near-to-failure event in ERCOT on February 26, 2008, is an example of such a situation [14]. Furthermore, the significant variations in active power flow into the system due to the proliferation of wind and PV could affect the electromagnetic torque-providing ability and thereby could have significant impact on rotor angle stability [13]. Therefore, the increased penetration of wind and PV in power systems has imposed the requirement that WPPs and PPPs should also contribute to the network support.

Manuscript received April 30, 2013; revised August 22, 2013 and October 21, 2013; accepted November 19, 2013. Date of publication December 11, 2013; date of current version April 16, 2014. Paper no. TPWRS-00535-2013.

N. Mithulananthan and R. Shah are with School of Information Technology and Electrical Engineering, The University of Queensland, Brisbane QLD-4072, Australia (e-mail: mithulan@itee.uq.edu.au; md.shah@uq.edu.au).

K. Y. Lee is with Department of Electrical and Computer Engineering, Baylor University, Waco, TX 76798-7356 USA (e-mail: Kwang_Y_Lee@baylor.edu).

Color versions of one or more of the figures in this paper are available online at http://ieeexplore.ieee.org.

Digital Object Identifier 10.1109/TPWRS.2013.2292615

The research efforts in [15] have been devoted to the design of power oscillation damping (POD) controller for wind generations. The authors in [16] have proposed a wide-area POD in PV for inter-area oscillation damping. There are some significant works regarding the coordinated design of POD for wind and synchronous generator in oscillation damping [17]. Most of these POD design techniques are based on advanced control techniques to ensure the robust performance of the controller under wide-range of uncertainties. However, these controllers are in higher order with complex structure. Even though the controllers are robust, the utilities would be reluctant to implement them in real power system since it is complex and capital intensive to be commissioned. Nonetheless, this POD technology is yet to be available in current DFIG and PV sold by manufacturer at present. On the other hand, it has been reported that the reactive power capability of DFIG and PV are under utilized in the current utility practice [18]–[20]. In the current industrial practice, the wind generators in power systems are allowed to operate at a fixed power factor (0.95 lead/lag) operation mode [21], and there is no specific grid code for reactive power operation of large-scale PVs. Current grid practice suggests that a large-scale PV plant might support the grid with very limited reactive power capability. By utilizing the built-in reactive power capabilities of renewable generation, the requirement placed on conventional generators could be eased and a secure system operation can be achieved.

From this perspective, this paper presents an operational planning methodology for small-disturbance angle stability control by utilizing the reactive power capability of renewable generators. The control action consists of setting different reactive power controls at selected sources (renewables) based on their influences on the small-disturbance angle stability. The method of changing the reactive power controls in renewable generations is referred to here as reactive power management. Additionally, the voltage stability assessment of the system has also been carried out to ensure that implementing the proposed reactive power control planning in renewable generations does not degrade the voltage stability of the system.

The remainder of this paper is organized as follows. Section II briefly describes the proposed operational planning methodology for small-disturbance angle stability control. In Section III, the mathematical formulation of structured singular value is presented. Detailed numerical results are presented in Section IV, and conclusions are drawn in Section V.

II. Methodology

Here, we briefly describe the reactive power management methodology for operational planning of power system from the point of view of small-disturbance angle stability.

A. Eigenvalue Sensitivity

Eigenvalue sensitivity analysis is employed in this paper to identify the critical renewable generation bus in terms of reactive power control in the system. The main constitution of this method is to combine the parameters corresponding to renewable reactive power control in such a way that their sensitivity reflects the importance of the reactive power control on the damping of electromechanical modes. The parameters used for the eigenvalue sensitivity analysis are: reactive power injection (Q) at renewable generator bus and the gain and time constant of the reactive current command control. Eigenvalue sensitivity of each inter-area mode is obtained for the above selected parameters. After calculating the sensitivity of inter-area modes for each parameter, the eigenvalue sensitivity index, referred to as the cumulative sensitivity index, is presented as the sum of the magnitudes of the sensitivities of all inter-area modes [10]. The adopted convention associates that the higher the value of cumulative sensitivity index is for the reactive power control parameters and reactive power injection, the more important is the renewable generator for reactive power control in terms of small-disturbance angle stability. Sensitivity analyses to each of the selected parameters are conducted for various operating conditions to confirm the robustness of the sensitivity index.

B. Clustering Method

Important renewable generator for reactive power management in terms of small-disturbance angle stability can be obtained from the above described eigenvalue sensitivity index. However, an unaddressed challenge is how many renewable generators should be considered for the specific reactive power control scheme, as there are no "cutoff" lines in the eigenvalue sensitivity-based index. Meanwhile, the inverter-based reactive power generation is cost-intensive as compared with the conventional methods of reactive compensation [19], [21]; the utility operation planner has to properly identify the critical renewable generations for reactive power control in terms of small-disturbance angle stability to justify the reactive power requirement other than the grid code for interconnection of wind and PV. Keeping this in consideration, this paper proposed a hierarchical principal component analysis (PCA) clustering method to identify the groups of coherent renewable generations. A similar reactive power control scheme would be applied to the renewable generators in a group. The clustering of renewable generators can be achieved by utilizing the PCA-based hierarchical clustering technique on the eigenvalue sensitivity indices.

PCA is a technique to transform the m correlated variables into a new set of uncorrelated variables known as principal components. If the data matrix X consists of m system variables measured for N samples, the full PCA decomposition converts the original $m \times N$ data matrix into the sum over m orthonormal basis functions as [22]

$$X = \begin{pmatrix} t_{1,1} \\ \vdots \\ t_{m,1} \end{pmatrix} w_1' + \ldots + \begin{pmatrix} t_{1,m} \\ \vdots \\ t_{m,m} \end{pmatrix} w_m' \tag{1}$$

where w_1' to w_m' represent principal components. The each principal component has $N \times 1$ dimension. The expression in (1) can be expressed in following compact matrix form:

$$X = TW'. \tag{2}$$

The elements of matrix T are known as t-scores or simply scores. This PCA decomposition can be easily obtained with

the help of the singular value decomposition (SVD) of data matrix X, which can be expressed as

$$X = USV' \tag{3}$$

where S is the singular value matrix of X, and U and V' are called the left-singular vector and right-singular vector, respectively. From (2) and (3), we identify $T = US$ and $W' = V'$. The ratio between the each eigenvalues of XX' and the sum of all eigenvalues provides a measure of the total variation by the corresponding eigenvectors or principal components [22]. The weight of the principal components can be represented graphically. If three w_i' are in use, the corresponding scores could be plotted in 3-D spanned by the three orthogonal principal components. However, this technique possesses inaccuracy in cluster identification since the clustering of the data depends on the visual inspection of the 3-D plot.

Therefore, in this paper, classification of the PCA has been done by utilizing hierarchical clustering method as proposed in [23]. Here, by evaluating the distance between objects, the clustering is acquired by merging clusters from the preceding level using similarity and/or dissimilarity measures as the basis of reference for clustering. A Euclidean norm [23], which is the usual measure of distance, is used here, which can be expressed as

$$d_{ij} = \sqrt{\sum_{k=1}^{m}(x_{ik} - x_{jk})^2} \tag{4}$$

where x_{ik} and x_{jk} are the values of the kth variable in the m-dimensional observation for individuals i and j, respectively. The distance measure d_{ij} is interpreted as the physical distance between the two points $x_i = (x_{i1}, \ldots, x_{im})$ and $x_j = (x_{j1}, \ldots, x_{jm})$ in Euclidean space. The physical distance between the nearest neighbors is obtained on the basis of *single linkage* clustering method [23].

In this paper, cumulative eigenvalue sensitivity index corresponding to 12 renewable generators are evaluated in 15 different operating conditions to form the data matrix for the PCA clustering. Then, their corresponding t-scores are used to build hierarchical clustering tree.

C. Reactive Power Management

Here, the underlying idea behind the reactive power management is explained from the theoretical view of structured singular value (SSV). The fundamental idea behind this approach is to control the robustness measure (μ) by varying reactive power control schemes of each renewable generation cluster with underlying uncertainties in the system. The methodology presented is built upon the method presented in [24].

System loads and renewable generation variations are considered as the underlying uncertainties for the process. The general practice in the SSV theory is to consider the uncertainties independently. Such an assumption could result in incomplete and unreliable small-disturbance angle stability characterization, especially for inter-area modes. Thus, a simultaneous method of considering uncertainties in the μ evaluation is used. Details about the SSV evaluation will be discussed later in the paper. The step-by-step methodology of the proposed operational planning is shown in the flowchart of Fig. 1.

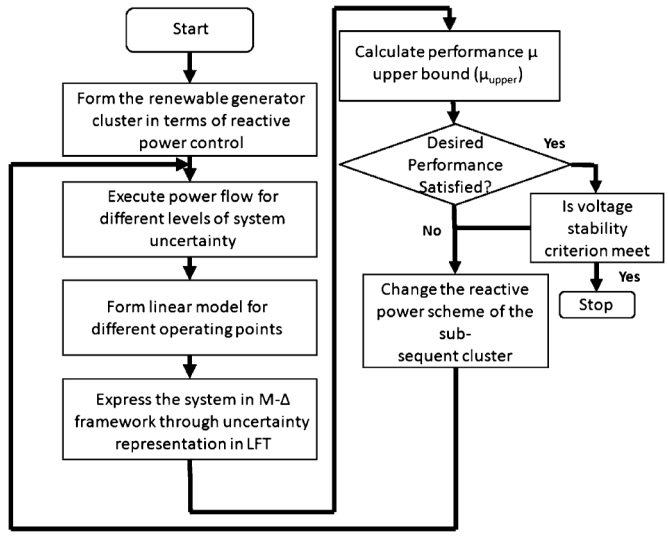

Fig. 1. Flowchart describing the process of reactive power management.

III. Formulation of Structured Singular Value

A. Perturbed State-Space Representation

The SSV theory has been successfully applied in large-scale power systems for robustness assessment and controller design [25]–[27]. The state-space realization of the general uncertain system can be expressed by

$$\dot{x} = A(p)x \tag{5}$$

where $p = [p_1, p_2, \ldots p_m]$ is the set of uncertain parameters, varied within certain ranges, and $A(p)$ is the parameter-dependent state matrix. Assuming that a parameter p_i has a nominal value p_{i0} and an uncertainty range $\pm r$, then the parametric uncertainty can be expressed by a parameter set as follows [25]:

$$p_i = \bar{p}_i(1 + r_i\delta_i), \quad i = 1, \ldots, m \tag{6}$$

where

$$\bar{p}_i = \frac{p_i^{\min} + p_i^{\max}}{2}, \quad r_i = \frac{p_i^{\max} - p_i^{\min}}{p_i^{\max} + p_i^{\min}}, \quad p_i \in [p_i^{\min}, p_i^{\max}].$$

$\bar{p}_i$ is the mean parametric value, r_i is the relative uncertainty in the parameter, and δ_i is a real scalar such that $-1 \leq \delta_i \leq 1$. From the above definition, the uncertain system representation can be expressed in terms of the nominal and perturbed parameters as follows:

$$\dot{x} = A(p)x = \left[A_0(p^0) + \sum_{i=1}^{m} A_i\delta_i\right] x \tag{7}$$

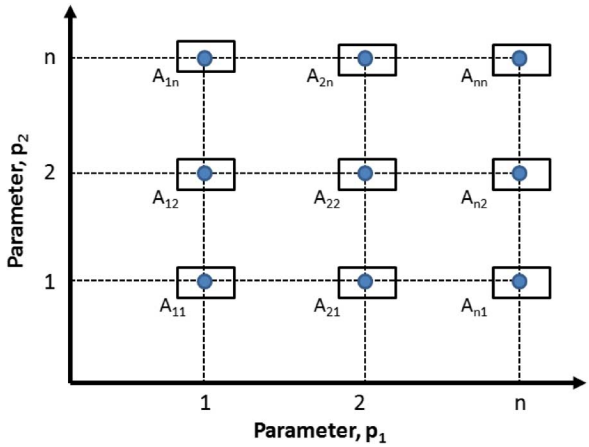

Fig. 2. Grid of operating conditions.

where A_0 represents the nominal plant, $p^0 = [p^0_{i1}, p^0_{i2}, \ldots, p^0_{im}]$ is the vector of uncertain parameters, and A_i matrices describe the deviation from the nominal system.

B. Description of Operating Space

For two varying parameters p_1 and p_2, assume that both parameters are varied simultaneously through the ranges of possible values, $p_1 = [p_{11}, p_{12}, \ldots, p_{1n}]$, $p_2 = [p_{21}, p_{22}, \ldots, p_{2n}]$, which gives a grid of n^2 operating conditions, as shown in Fig. 2. The load flow and small-signal analyses for n^2 operating conditions are performed to evaluate the dependency of the elements of state matrix A on the varying parameters. Once the parameter-dependent state matrix for multiple conditions have evaluated, the variation of the coefficient a_{ij} of each state matrix A is approximated by a nonlinear relationship $a^{\text{var}}_{ij} = f_{ij}(p_1, p_2)$ and can be expressed by the second-order polynomial approximation as follows:

$$a^{\text{var}}_{ij} = \hat{a}_{ij0} + \hat{a}_{ij1}p_1 + \hat{a}_{ij11}p_1^2 + \hat{a}_{ij2}p_2 + \hat{a}_{ij22}p_2^2 + \hat{a}_{ij12}p_1p_2 \tag{8}$$

The polynomial in (8) can be solved by the over determined set of linear equation as

$$X\hat{a} = y \tag{9}$$

where X represents the matrix of uncertainties, $\hat{a}$ represents unknown parameter vector, and y is the vector corresponding to the varying elements of state matrices. Equation (9) describes a set of simultaneous algebraic equations, and the solution of the unknown vector $\hat{a}$ can be obtained by the following least square solution:

$$\hat{a} = X^+ y = \left(X^T X\right)^{-1} X^T y \tag{10}$$

where X^+ represents the Moore–Penrose pseudo-inverse of uncertainty matrix X. Once $\hat{a}$ is obtained from (10), the next step is to obtain the parametric uncertainty description for the system and uncertainties through linear fractional transformation (LFT). A detail on LFT representation is depicted next.

C. Linear Fractional Transformation (LFT) Representation

The LFT provides a common framework for the evaluation of stability robustness and performance with uncertainty [25]. In order to generate LFT, all of the uncertainties in the system need to be represented in a diagonal uncertainty matrix Δ. For a system with two varying parameters, the element a_{ij} of system matrix with structured uncertainty can be expressed as

$$a^{\text{var}}_{ij} = a_{ij0} + a_{ij1}\delta_1 + a_{ij11}\delta_1^2 + a_{ij2}\delta_2 + a_{ij22}\delta_2^2 + a_{ij12}\delta_1\delta_2. \tag{11}$$

Having repeated the above mentioned routine for all of the varying elements of the state matrix A, the following state-space realization can be obtained:

$$\begin{bmatrix} \dot{x} \\ y \end{bmatrix} = \begin{bmatrix} (A_0 + \Delta A) & B \\ C & D \end{bmatrix} \begin{bmatrix} x \\ u \end{bmatrix} \tag{12}$$

where

$$\begin{aligned}(A_0 + \Delta A) =& A_0^{\text{var}} + L^T \left[A_1^{\text{var}}(\delta_1 I) + A_{11}^{\text{var}}\left(\delta_1^2 I\right)\right. \\ &\left. + A_2^{\text{var}}(\delta_2 I) + A_{22}^{\text{var}}\left(\delta_2^2 I\right) + A_{12}^{\text{var}}(\delta_1\delta_2 I)\right] R.\end{aligned}$$

Here, A_0 represents the nominal plant and the matrices A_0^{var}, A_1^{var}, A_{11}^{var}, A_2^{var}, A_{22}^{var}, and A_{12}^{var}, respectively, account the changes in (i, j) entries of linearized power system model. L and R are the matrices with 0's and 1's and relate to the change of system matrix rows and columns with operating conditions.

The system in (12) can be construed into the robustness analysis framework. To separate the nominal transfer function and uncertainty elements, additional fictitious inputs and outputs are considered. Following the approach of [25], the system in (12) can be expressed as

$$\begin{bmatrix} \dot{x} \\ z \end{bmatrix} = \begin{bmatrix} A_0 & A_1^{\text{var}} & \ldots & A_n^{\text{var}} \\ R & 0 & \ldots & 0 \\ 0 & I & \ldots & 0 \\ R & 0 & \ldots & 0 \\ 0 & I & \ldots & 0 \end{bmatrix} \begin{bmatrix} x \\ W \end{bmatrix} \tag{13}$$

where W and z are the inputs and outputs to the uncertainties, respectively. Based on the above LFT-uncertainty, the system in (13) can be written in the typical matrix forms as follows:

$$\dot{x} = M_{11}(s)x + M_{12}(s)W \tag{14}$$

$$z = M_{21}(s)x + M_{22}(s)W \tag{15}$$

$$W = \Delta(\delta)z$$

where $\Delta(\delta)$ has the diagonal structure, $\Delta(\delta) = blockdiag(\delta_1 I, \delta_{11}^2 I, \ldots)$. Now, the resulting closed-loop system can be expressed by the upper LFT of M closed-loop system with Δ as

$$\dot{x} = F_u\left(M, \Delta(\delta)\right)x, \quad \forall \Delta \in \Delta \tag{16}$$

where $F_u(M, \Delta(\delta))$ is the upper LFT of the uncertain system and can be expressed as

$$F_u\left(M, \Delta(\delta)\right) = M_{22} + M_{21}\Delta(\delta)\left(I - M_{11}\Delta(\delta)\right)^{-1} M_{12}. \tag{17}$$

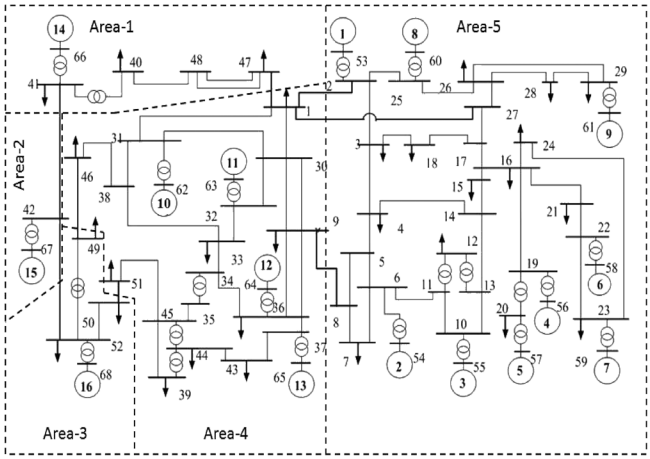

Fig. 3. Single-line diagram of the 16-machine 68-bus test system.

Having the LFT-based uncertainty model of the underlying system, robust stability can be estimated by applying the μ analysis. The system under consideration is called robustly stable for all Δ with $\|\Delta\|_\infty \leq 1$ if M is stable and $F_\mu(M, \Delta(\delta))$ stays in a H_∞ norm bounded by the unity (i.e.,$\mu_\Delta < 1$).

IV. Case Studies

A. Test System

The 16-machine 68-bus test system was used in this analysis, as shown in Fig. 3. It is an interconnected test system of New England (NEST) and New York power system (NYPS) with five areas. The general description of the system is given in [28]. For this analysis, the sixth-order synchronous generator model has been considered for all generators of the system. The dynamic system data and the nominal power transfer between the areas are available in [28]. For small-disturbance angle stability analysis, the load of the system was modeled as static load to include 33% constant current, 33% constant impedance, and 33% constant power [29].

WPPs and PPPs are integrated to the system buses listed in Table I. The locations of these generators are chosen to reflect the realistic distribution of renewables in the power system; hence, WPPs and PPPs are located near the load center, generators and remote areas of the system. The penetration of 20% (4200 MW for a load level of 21 000 MW) is considered for the analysis. A generic model of Type-3 wind turbine (DFIG) and PV are used [30], [31] in this paper. Detailed descriptions of these generic models can be found in [30] and [31]. These generators have the capability of controlling reactive power in the following ways: extended capability curve operation, voltage control mode operation, power factor control mode operation, and fixed reactive power operation. For this study, extended capability curve, voltage control mode, and power factor mode operations are considered as the available reactive power control schemes in WPPs and PPPs.

TABLE I
Renewable Generator Locations

Generator type	Connection Bus
DFIG	6,8,14,16,33,40
PV	3,5,30,31,38,48

TABLE II
Scenarios for Small-Disturbance Angle Stability Analysis

Scenarios	I	II	III	IV	V	VI
DFIG output levels (%)	45	75	65	50	55	85
PV output levels (%)	45	50	65	75	85	55
Load levels (GW)	18.6	18.2	19.1	17.1	17.6	19.6

TABLE III
Inter-Area Modes of the Systems

Scenarios		I	II	III	IV	V	VI
Mode-1	%ζ	10.5	8.9	10.8	8.7	9.01	9.6
	f(Hz)	0.35	0.38	0.36	0.42	0.404	0.402
Mode-2	%ζ	9.8	9.6	9.15	9.2	9.2	9.6
	f(Hz)	0.48	0.51	0.50	0.53	0.54	0.5
Mode-3	%ζ	5.6	5.4	5.8	5.04	5.3	4.5
	f(Hz)	0.62	0.63	0.58	0.62	0.62	0.64
Mode-4	%ζ	8.01	7.6	8.03	7.8	7.9	7.8
	f(Hz)	0.72	0.73	0.73	0.74	0.73	0.76

B. Assessment of Small-Disturbance Angle Stability

Here, the impact of DFIG and PV generation on power-system small-disturbance angle stability will be illustrated. For analysis, 0.95 lead/lag operation of DFIG is considered while, for PV, 0.98 leading power factor operation has been adopted. One major aspect regarding the integration of DFIG and PV to the system is the de-commissioning of the conventional generations with auxiliary support to the system. To accommodate the DFIG and PV to this system, the generators 8 and 9 in the system (Fig. 3) are physically replaced. Table II depicts the different operating scenarios, covering from low to high load conditions with various output levels of DFIG and PV, which are considered for small-disturbance angle stability analysis.

Table III shows the percentage of damping and frequency of oscillations for the four inter-area modes (referred as modes 1–4 henceforth) of the system corresponding to the operating conditions given in Table II. The frequencies of the inter-area modes are lying between 0.35–0.76 Hz. From the table, it is evident that, at some operating conditions, the damping of the inter-area modes experienced an adverse effect, while some other modes experienced a beneficial effect on the specific operating conditions. From the table, it is also clear that mode 3 is affected most due to the integration of DFIGs and PVs to the system. It is worth noting that the frequencies of inter-area modes are significantly affected due to the de-commissioning of synchronous generators 8 and 9.

TABLE IV
EIGENVALUE SENSITIVITY ANALYSIS

RG No.	Bus No.	$\sum_{i=1}^{n}\left\|\frac{\partial\lambda_i}{\partial Q}\right\|$	$\sum_{i=1}^{n}\left\|\frac{\partial\lambda_i}{\partial K_Q}\right\|$	$\sum_{i=1}^{n}\left\|\frac{\partial\lambda_i}{\partial T_Q}\right\|$	Cumulative index	Ranking
1	3	0.0046	0.00125	0.00021	0.0060	9
2	5	0.0049	0.00126	0.00112	0.0073	8
3	6	0.0146	0.00024	0.00119	0.0161	4
4	8	0.0032	0.00081	0.0005	0.0045	12
5	14	0.0127	0.0031	0.00141	0.0172	3
6	16	0.0249	0.0170	0.00178	0.0440	1
7	30	0.0037	0.00017	0.00078	0.0047	11
8	31	0.0055	0.0012	0.00087	0.0076	7
9	33	0.0082	0.00457	0.00107	0.0141	5
10	38	0.0038	0.00059	0.00044	0.0049	10
11	40	0.0207	0.01230	0.00176	0.0342	2
12	48	0.0112	0.00065	0.00029	0.0123	6

C. Reactive Power Control Allocation

As per the illustrated method in Section II-A, the cumulative eigenvalue sensitivity indices have been used to identify the important renewable generator locations for reactive power management in terms of small-disturbance angle stability. Sensitivity analysis has been performed for each selected parameter variation corresponding to inter-area modes of oscillation and finally, the cumulative eigenvalue sensitivity index is represented as the sum of the magnitudes of the eigenvalue sensitivities for all inter-area modes corresponds to all parameter variations. Eigenvalue sensitivity analysis has been carried out for all six operating scenarios to confirm the robustness of the indices. Finally, the mean values of the eigenvalue sensitivity indices shown in Table IV have been utilized to identify important renewable generators in the system. In Table IV, column three represents the sum of the magnitudes of inter-area mode sensitivities with respect to renewable reactive power injection, while columns four and five represent the sum of the magnitudes of inter-area mode sensitivities with respect to gain and time constant of renewable reactive power controls, respectively. Column six represents the cumulative sensitivity indices for all renewable generators, which determines the rankings of the renewable generators shown in column seven. From the results in Table IV, it can be seen that renewable generator at bus 16 is most important for reactive power control in terms of small-disturbance angle stability, while reactive power control of the renewable generator at bus 8 has the least influence on small-disturbance angle stability.

The eigenvalue sensitivity indices are used to find the cluster of renewable generators for reactive power control as per the method illustrated in Section II-B. Fig. 4 shows the renewable generator clusters based on the hierarchical PCA-based clustering. An intermediate link has been chosen to form the cluster of the renewable generators. From the figure it is evident that if one has considered the intermediate link (Euclidean distance of 1.70) for clustering, the renewable generators can be grouped into six clusters which are: {6}, {11}, {3, 5}, {9, 12}, {8}, and {the rest of the renewable generators: 1, 2, 4, 7, 10}. Summary of clustering for WPPs and PPPs are given in Table V.

Variability in PV and wind generation output as well as loads are considered in the structured singular value

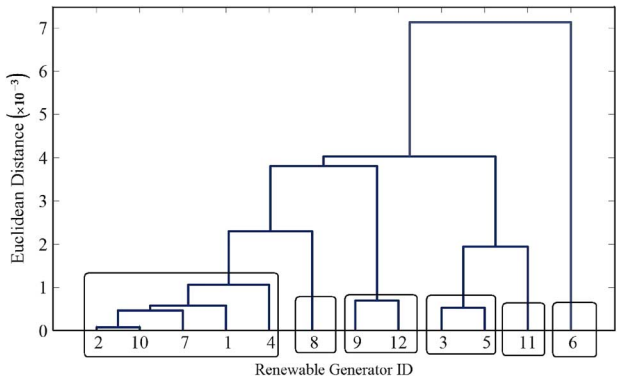

Fig. 4. Hierarchical PCA clustering of renewable generation.

TABLE V
SUMMARY OF CLUSTERING FOR RENEWABLE GENERATIONS

Group	Renewable Generator ID	Renewable Generator Bus
Group-1	{6}	{16}
Group-2	{11}	{40}
Group-3	{3,5}	{6,14}
Group-4	{9,12}	{33,48}
Group-5	{8}	{31}
Group-6	{1,2,4,7,10}	{3,5,8,30,38}

TABLE VI
SELECTED CONVENTIONAL GENERATOR OUTPUTS

Bus no.	Generator no.	Adjustable Generator Outputs (MW)
63	11	[705-1200]
64	12	[1020-1690]
68	16	[3000-3820]
56	4	[497-696]
58	6	[565-820]
62	10	[685-980]

formulation. For SSV analysis, vector of loads, $P1 = [16\text{ GW}, 18\text{ GW}, 21\text{ GW}]$ and vector of renewable generations, $P2 = [2600\text{ MW}, 3000\text{ MW}, 3400\text{ MW}]$ have been used. In SSV formulation, generators 8 and 9 in buses 60 and 61, respectively, are physically de-commissioned to integrate renewable generators. For this analysis, corresponding to the renewable generator outputs, the conventional generator outputs at some selected buses have been varied as shown in Table VI. The corresponding conventional generators have been selected by generator ranking index as described in [10]. The amount of variations in the selected conventional generator outputs are governed by the cost function of the particular generator and the deviation of renewable power generations.

The results in Fig. 5 show the μ upper bound at final iteration for the frequency range associated with the inter-area modes of the system. From the results in Fig. 5 the maximum value of $\mu(\mu = 0.63)$ indicates that the system is stable for the whole operating space considered for the analysis. Table VII shows the employed reactive power control scheme at renewable generator clusters in the final step of the SSV analysis.

Fig. 6 shows the eigenvalue analysis for electromechanical modes in two different output levels of renewables for high

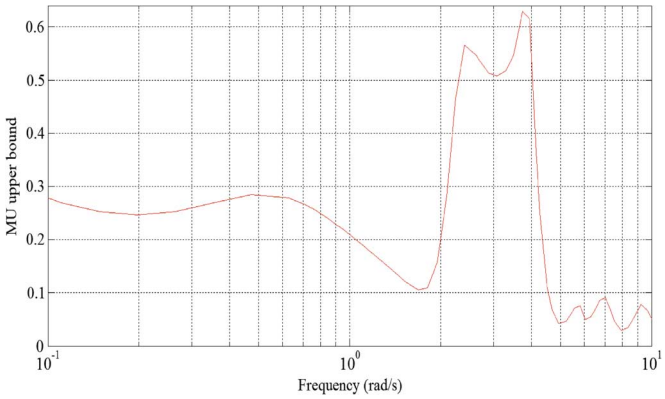

Fig. 5. The μ upper bound for the test system.

TABLE VII
REACTIVE POWER CONTROL SCHEME (FINAL ITERATION)

Group	Reactive Power Control Scheme
Group-1	Extended capability curve operation
Group-2	Extended capability curve operation
Group-3	Voltage control mode
Group-4	Power factor control mode (0.92 lead/lag power factor)
Group-5	Power factor control mode (0.93 lead/lag power factor)
Group-6	Power factor control mode (0.94 lead/lag power factor)

and low load conditions, 21 and 16 GW. From the figure, it is clear that the critical inter-area modes of the systems are well damped and satisfies the utility practice of system operation from the view point of small-disturbance angle stability. Table VIII summarized the percentage of damping, frequency of oscillations, and the percentage of change of damping in four inter-area modes after the implementation of renewable reactive power management for the system operating conditions presented in Table II. From the results in Table VIII, it can be seen that all of the inter-area modes have experienced beneficial effect with the proposed reactive power management.

D. Voltage Stability Analysis

Once the desired μ *upper bound* has been obtained (less than 1) and the damping performance is checked, the next step is to analyze the voltage stability of the system to ensure that the selected implementation of reactive power control does not degrade the overall voltage stability performance of the system. First, the steady-state analysis is conducted to evaluate the static voltage performance of the system. Steady-state analysis has been conducted for the system load model consisting of 33% constant power, 33% constant current, and 33% constant impedance. The analysis has been done for several severe contingency cases. Since the conventional generators near the load centers in area-5 are replaced by the WPPs and PPPs, the P-V curve of the load buses in area-5 is monitored for severe contingency cases. There are three low voltage load buses in area-5 of the system; for brevity, the P-V curve of the lowest voltage bus (bus 29) for the most severe contingency case (outage of the line between buses 38 and 46) is shown in Fig. 7. From the results in Fig. 7 it is evident that the system shows

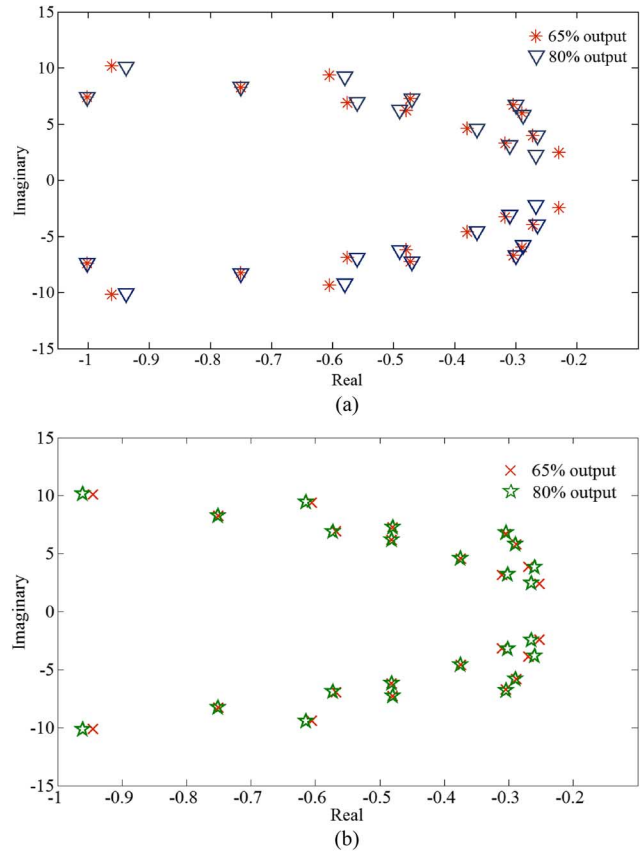

Fig. 6. System electromechanical modes: (a) high-load condition and (b) low-load condition.

TABLE VIII
SYSTEM INTER-AREA MODES WITH PROPOSED REACTIVE POWER MANAGEMENT

Scenarios		I	II	III	IV	V	VI
Mode-1	%ζ	11.9	10.5	12.1	9.14	9.4	10.85
	f(Hz)	0.35	0.38	0.36	0.42	0.404	0.402
	% Δ ζ	1.4	1.6	1.3	0.44	0.39	1.25
Mode-2	%ζ	9.8	9.8	10.5	9.7	9.75	10
	f(Hz)	0.48	0.51	0.50	0.53	0.54	0.5
	% Δ ζ	0	0.2	1.4	0.5	0.55	0.4
Mode-3	%ζ	7.6	7.3	7.89	7.02	7.2	7.1
	f(Hz)	0.62	0.63	0.58	0.62	0.62	0.64
	% Δ ζ	1.9	1.9	2.09	1.98	1.9	2.6
Mode-4	%ζ	8.03	8.21	8.1	8.2	8.3	8.1
	f(Hz)	0.72	0.73	0.73	0.74	0.73	0.76
	% Δ ζ	0.02	0.61	0.07	0.4	0.4	0.3

better steady state voltage performance with the proposed reactive power management in renewable generators.

Later, a short-term dynamic voltage stability analysis is conducted for the most severe contingency case obtained from the steady-state analysis in order to ensure that the proposed renewable reactive power management method does not degrade the dynamic voltage performance of the system. Since the short-term voltage stability is on the study of load response corresponding to a fault, an accurate representation of the system load is sought. Thereby, for short-term voltage stability analysis, the

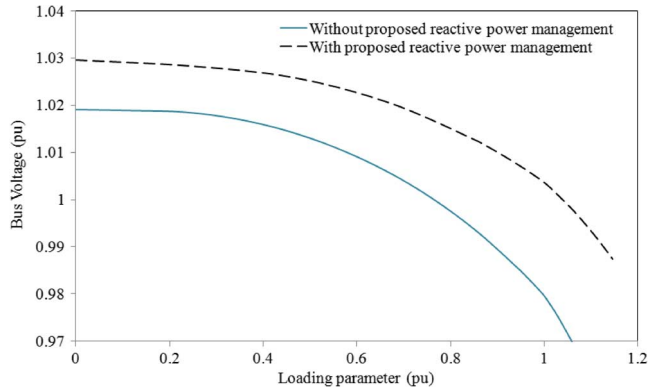

Fig. 7. P-V analysis results for a severe $N-1$ contingency (Bus 29).

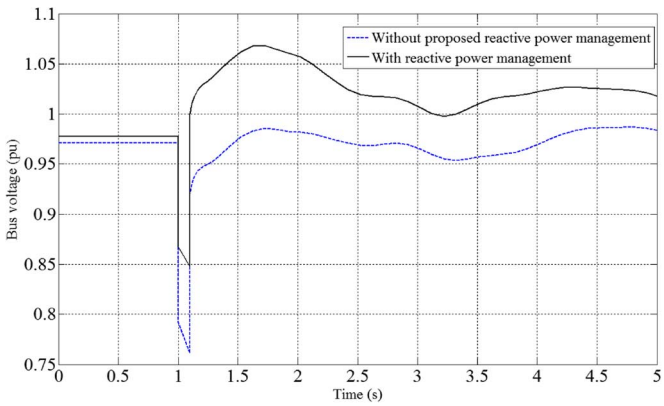

Fig. 8. Voltage of bus 71 with 80% renewable generator outputs.

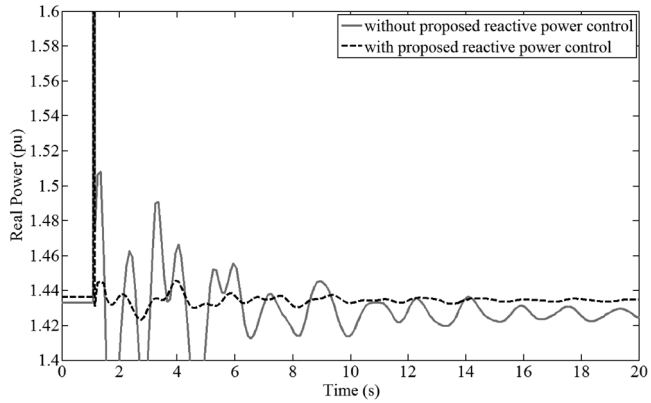

Fig. 9. Power-flow-response time-domain simulation.

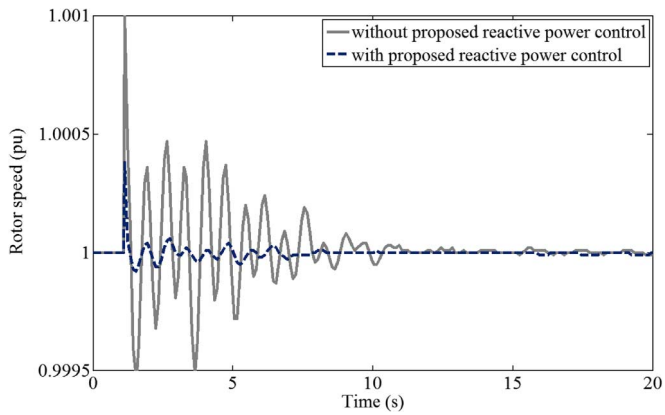

Fig. 10. Machine-speed time-domain simulation (Generator 1).

load buses 26, 28, and 29 are stepped down to subtransmission voltage level, and the new subtransmission voltage buses are assigned numbers 69–71. To capture the accurate load behavior, the loads are modeled to include 45% motor load and 55% static load [32], [33]. The active components of the static load are represented as constant current model and the reactive components as constant impedance, as recommended in [29]. For short-term voltage stability analysis, a three-phase self-clearing fault is applied near bus 29 for 100 ms. Voltage of bus 71 (subtransmission bus connected to bus 29) is monitored and recorded for heavy system load condition (21 GW) at 80% renewable generation outputs. According to NERC criteria for WECC system, after the disturbance, voltage magnitude dip and swell should not exceed its nominal value by 20% and 25%, respectively, for more than 20 cycles (0.33 s) [34]. From Fig. 8 it can be seen that after disturbance, voltage magnitude dip and swell of bus 71 does not exceed its nominal value by 20% and 25%, respectively, for more than 20 cycles, hence, in compliance with the NERC criteria for short-term voltage stability.

E. Transient Analysis

The transient analysis was performed for the medium load level of 18 GW. This has been done in order to confirm that the linear analysis results hold true in the presence of nonlinearity. For transient analysis, a three-phase fault is applied near bus 37 for 100 ms. In Fig. 9, the resulting deviation of active power in the tie-line between buses 38–46 is shown before and after the implementation of the renewable reactive power control scheme. From the figure, it can be seen that the proposed reactive power control at renewable generations responded well to the power oscillations that occur in the test system. The tie-line power oscillation is settled in approximately 12–14 s. Since 10–20 s of settling time is used by most utilities in their system operation [35], [36], it can be concluded that the proposed operational planning methodology for small-disturbance angle stability settles the oscillation within the desired time frame. Moreover, it is evident from the results that the tie-line oscillation decays faster with the proposed renewable reactive power control.

Fig. 10 shows the rotor speed of generator 1 (bus 53, area-5) before and after the implementation of the proposed reactive power control at renewable generators. From the figure, it is noticeable that the rotor speed of generator 1 showed much lower excursion for the proposed reactive power control at renewable generators, resulting in faster oscillation decay, thereby indicating a satisfactory performance of the proposed algorithm.

F. Dynamic Transfer Capability

Transfer capability of the power system defines how much the tie-line power between areas can be increased without compromising the system stability/security [37]. A system with large inter-area transfers is generally more robust and flexible in view of system security compared with the system with limited transfer capability [38], [39]. Thereby, the dynamic transfer capability of the system can be a useful measure to

TABLE IX
DYNAMIC TRANSFER CAPABILITY WITH AND WITHOUT PROPOSED REACTIVE POWER MANAGEMENT†

	Without proposed reactive power control	With proposed reactive power control
Dynamic Transfer capability (MW)	469.17	504.46

† On the line between buses 1 and 2 for areas 4 and 5, respectively.

indicate the merits of the proposed renewable reactive power control. A number of methods to evaluate available transfer capability have been reported in the literature. In his paper, the method proposed in [38] has been considered for transfer capability computation. The variation of dynamic transfer capability before and after the implementation of the proposed reactive power control at renewable generators is illustrated in Table IX for the line between buses 1 and 2 for areas 4 and 5, respectively. From the table, it is evident that, after the implementation of the proposed reactive power control at renewable generators, the available transfer capability for the line between buses 1–2 has increased significantly (from 469.17 to 504.46 MW), indicating the benefit of the proposed reactive power control scheme.

V. CONCLUSION

This paper has demonstrated the feasibility of using the built-in capability of renewable generators for small-disturbance angle stability control. The proposed methodology is based on the reactive power management of renewable generators other than the grid code. For implementing the reactive power control scheme, clusters of renewable generators have been formed based on the hierarchical PCA method. Specific reactive power control scheme has been implemented to the renewable generators in those clusters and the SSV analysis has been performed to verify the system robust stability with the adopted reactive power control scheme on the renewables. The case studies show that the adopted planning mechanism can maintain the small-disturbance angle stability of the system for a wide range of system operating conditions. In addition, voltage stability analysis results reveal that implementing the proposed renewable reactive power control scheme does not degrade the static and dynamic voltage performance of the system.

REFERENCES

[1] "Top 50 large-scale photovoltaic power plants," [Online]. Available: http://www.pvsources.com

[2] "A report by European Wind Energy Association," EU Energy Policy to 2050, Mar. 2011.

[3] "Photovoltaic power systems programme, trends in photovoltaic applications-Survey report of selected IEA countries between 1992 and 2008," Int. Energy Agency, IEA-PVPS T1-18:2009, 2009.

[4] "Renewable energy policy network for the 21st century," Renewables 2011: Global Status Rep., Sep. 2011 [Online]. Available: http://www.ren21.net

[5] "Renewable portfolio standards fact sheet," US Environmental Protection Agency, 2009 [Online]. Available: http://www.epa.gov/chp/statepolicy/renewable_fs.html

[6] D. Thakur and N. Mithulananthan, "Influence of constant speed wind turbine generator on power system oscillation," *Electr. Power Compon. Syst.*, vol. 37, no. 5, pp. 478–494, 2009.

[7] J. G. Slootweg and W. L. Kling, "The impact of large scale wind power generation on power system oscillations," *Electr. Power Syst. Res.*, vol. 67, no. 1, pp. 9–20, 2003.

[8] D. Gautam, V. Vittal, and T. Harbour, "Impact of increased penetration of DFIG-based wind turbine generators on transient and small signal stability of power systems," *IEEE Trans. Power Syst.*, vol. 24, no. 3, pp. 1426–1434, Aug. 2009.

[9] W. Du, H. F. Wang, and L.-Y. Xiao, "Power system small-signal stability as affected by grid-connected photovoltaic generation," *Eur. Trans. Electrical Power*, vol. 21, no. 5, pp. 688–703, Jul. 2011.

[10] R. Shah, N. Mithulananthan, and R. C. Bansal, "Oscillatory stability analysis with high penetrations of large-scale photovoltaic generation," *Energy Conv. Manag.*, vol. 65, pp. 420–429, Jan. 2013.

[11] T. Ackermann, *Wind Power in Power Systems*. Chichester, U.K.: Wiley, 2012.

[12] "Power electronics for wind turbine," [Online]. Available: http://www.i_micronews.com/upload/Rapport/Yole_Super_Wind-turbine_sample_January2012.pdf

[13] D. Gautom, "Impact of increased penetration of DFIG based wind turbine generators on rotor angle stability of power system," Ph.D dissertation, Dept. Electr. Eng., Arizona State Univ., Phoenix, AZ, USA, 2010.

[14] E. Ela and B. Kirby, "ERCOT event on February 26, 2008: Lessons learned," NREL, Rep. NREL/TP-500-43373, 2008.

[15] F. M. Hughes, O. A. Lara, N. Jenkins, and G. Strbac, "Control of DFIG based wind generation for power network support," *IEEE Trans. Power Syst.*, vol. 20, no. 4, pp. 1958–1966, Nov. 2005.

[16] R. Shah, N. Mithulananthan, and K. Y. Lee, "Large-scale PV plant with a robust controller considering power oscillation damping," *IEEE Trans. Energy Conv.*, vol. 28, no. 1, pp. 106–116, Mar. 2013.

[17] H. Huang and C. Y. Chung, "Coordinated damping control design for DFIG-based wind generation considering power output variation," *IEEE Trans. Power Syst.*, vol. 27, no. 4, pp. 1916–1925, Nov. 2012.

[18] M. Kayikci and J. V. Milanovic, "Reactive power control strategies for DFIG-plants," *IEEE Trans. Energy Conv.*, vol. 22, no. 2, pp. 389–396, Jun. 2007.

[19] R. Konopinski, P. Vijayan, and V. Ajjarapu, "Extended reactive capability of DFIG wind parks for enhanced system performance," *IEEE Trans. Power Syst.*, vol. 24, no. 3, pp. 1346–1355, Aug. 2009.

[20] K. K. Yagnik and V. Ajjarapu, "Consideration of wind and solar generation reactive power capability on grid voltage performance," in *Proc. IEEE Power and Energy Soc. General Meeting*, San Diego, CA, USA, Jul. 22–26, 2012.

[21] "FERC Standard Large Generator Interconnection Agreement (LGIA)," Jun. 16, 2005 [Online]. Available: http://www.ferc.gov/industries

[22] N. F. Thornhill, "Spectral principal component analysis of dynamic process data," *Control Eng. Practice*, vol. 10, no. 8, pp. 833–846, Aug. 2002.

[23] B. S. Everitt, *Cluster Analysis*. London, U.K.: Edward Arnold, 1993.

[24] B. Ramanathan and V. Vittal, "Small-disturbance angle stability enhancement through direct load control—Part I: Framework development," *IEEE Trans. Power Syst.*, vol. 21, no. 2, pp. 773–781, May 2006.

[25] R. B. Castellanos, A. R. Messina, and H. U. Sarmiento, "A μ-analysis approach to power system stability robustness evaluation," *Electr. Power Syst. Res.*, vol. 78, pp. 192–201, 2008.

[26] H. Nguyen-Duc, L. Dessaint, and A. Okou, "Power system robust stability analysis using structured singular value theory and model reduction method," in *Proc. IEEE Power and Energy Soc. Gen. Meeting*, 2009, pp. 1–6.

[27] M. Rios, N. Hadjsaid, R. Feuillet, and A. Torres, "Power systems stability robustness evaluation by μ analysis," *IEEE Trans. Power Syst.*, vol. 4, no. 2, pp. 648–653, May 1999.

[28] G. Rogers, *Power System Oscillations*. Boston, MA, USA: Kluwer Academic, 2000.

[29] IEEE Task Force on Load Representation for Dynamic Performance, "Standard load models for power flow and dynamic performance simulation," *IEEE Trans. Power Systems*, vol. 10, no. 3, pp. 1302–1313, Aug. 1995.

[30] Generic Type-3 Wind Turbine-Generator Model for Grid Studies. ver. 1.1, WECC Wind Generator Modelling Group, Sep. 2006.

[31] K. Clark, M. W. Miller, and R. Walling, *Modeling of GE Solar Photovoltaic Plants for Grid Studies*. Schenectady, NY, USA: General Electric Int. Inc., 2009.

[32] J. A. Diaz de Leon, II and B. Kehrli, "The modelling requirement for shortterm voltage stability studies," in *Proc. IEEE PES Power Syst. Conf. Exposition*, Oct. 29–Nov. 1, 2006, pp. 582–588.

[33] "Voltage stability assessment: Concepts, practice and tools," in *Proc. IEEE PES Power System Stability Sub-Committee Special Publication*, Aug. 2004, Final Document.
[34] A. M. Abed, "WSCC voltage stability criteria, under voltage load shedding and reactive power reserve monitoring methodology," in *Proc. IEEE PES-Summer Meeting*, 1999, pp. 191–197.
[35] J. Paserba, "Analysis and control of power system oscillation," CIGRE, CIGRE special pub. 38.01.07, 1996.
[36] B. Pal and B. Chaudhuri, *Robust Control in Power Systems*. New York, NY, USA: Springer, 2005.
[37] North Amer. Electric Reliability Council (NERC), "Available transfer capability definitions and determination," Jun. 2000.
[38] M. J. Hossain, "Dynamic voltage stability augmentation in interconnected power systems with renewable energy," Ph.D dissertation, Sch. Eng. Inf. Technol., Univ. of New South Wales, Queensland, Australia, Nov. 2010.
[39] Y. Cheng, T. S. Chung, C. Y. Chung, and C. W. Yu, "Dynamic voltage stability constrained ATC calculation by a QSS approach," *Int. J. Electr. Power Energy Syst.*, vol. 28, no. 6, pp. 408–412, Jul. 2006.

Nadarajah Mithulananthan (SM'10) received the Ph.D. degree in electrical and computer engineering from University of Waterloo, Waterloo, ON, Canada, in 2002.

He was an Electrical Engineer with the Generation Planning Branch, Ceylon Electricity Board, Sri Lanka, and a Researcher with Chulalongkorn University, Bangkok, Thailand. He also served as an Associate Professor with the Asian Institute of Technology, Bangkok, Thailand. He is currently a Senior Lecturer with the University of Queensland, Brisbane, Australia. His main research interests are voltage stability and oscillation studies on practical power systems, application of FACTS controller, and renewable energy technology.

Rakibuzzaman Shah (S'10) received the B.Sc.Eng. degree in electrical and electronic engineering from Khulna University of Engineering & Technology (KUET), Khulna, Bangladesh, and the M.Eng. degree in energy from the Asian Institute of Technology, Bangkok, Thailand, in 2005 and 2009, respectively. He is currently working toward the Ph.D. degree at the University of Queensland, Brisbane, Australia.

His main research interests are power system stability, renewable energy technology, control application in power system, and power system interconnection issues.

Kwang Y. Lee (F'01) received the B.S. degree in electrical engineering from Seoul National University, Seoul, Korea, in 1964, the M.S. degree in electrical engineering from North Dakota State University, Fargo, ND, USA, in 1968, and the Ph.D. degree in system science from Michigan State University, East Lansing, MI, USA, in 1971.

He has been on the faculties of Michigan State, Oregon State, Houston, the Pennsylvania State University, and Baylor University, where he is currently a Professor and Chair of the Electrical and Computer Engineering and Director of the Power and Energy Systems Laboratory. His research interests are power systems control, operation and planning, and intelligent systems applications to power plants and power systems control.

Dr. Lee has served as an editor of the IEEE TRANSACTIONS ON ENERGY CONVERSION and an associate editor of the IEEE TRANSACTIONS ON NEURAL NETWORKS. He is currently serving as Chair of the IEEE Working Group on Modern Heuristic Optimization and Chair of the IFAC Working Group on Smart Grids.